JES Focus Issue on Mathematical Modeling of Electrochemical Systems at Multiple Scales in Honor of John Newman

Model Based Analysis of One-Dimensional Oriented Lithium-Ion Battery Electrodes

Tandeep S. Chadha,[a] Bharatkumar Suthar,[a,*] Derek Rife,[a] Venkat R. Subramanian,[b,] and Pratim Biswas[a,z]**

[a]*Aerosol and Air Quality Research Laboratory, Department of Energy, Environmental and Chemical Engineering, Washington University in St. Louis, St. Louis, Missouri 63130, USA*
[b]*Department of Chemical Engineering, University of Washington, Seattle, Washington 98195, USA*

Oriented one-dimensional nanostructures have been of substantial interest as electrodes for lithium-ion batteries due to the better performance both in terms of initial capacity and lower capacity fade compared to powder pressed electrodes. This paper focuses on a model driven approach to understanding the relationship between the morphology of these oriented nanostructures to the performance of the battery. The Newman-type P2D modeling technique is applied to a porous electrode made up with solid continuous cylinders that extends from the current collectors to separator. TiO_2 columnar nanostructures of varying heights were synthesized using the aerosol chemical vapor deposition (ACVD) and their performance as electrodes in a lithium-ion battery was measured. This electrochemical transport model was validated with the experimental data. This model was used to understand the role of transport parameters, including the diffusivity of lithium in the TiO_2 and the electronic conductivity of the TiO_2 columns, and structural parameters, including the height of the columns and the porosity of the electrode, on the areal capacity of a lithium ion battery at different rates of discharge. The model enables for the prediction of optimized structural parameters of one-dimensional electrodes tailored to the desired application of lithium and sodium-ion batteries.

Manuscript submitted March 6, 2017; revised manuscript received April 21, 2017. Published May 4, 2017. *This paper is part of the JES Focus Issue on Mathematical Modeling of Electrochemical Systems at Multiple Scales in Honor of John Newman.*

Lithium-ion batteries (LiBs) have emerged as the dominant power source for most electronic applications today, as well as the most suitable candidates for electric vehicles and hybrid electric vehicles. The diverse range of applications for which LIBs are used demand both high energy densities and high power densities, although they are inversely related.[1] Several research approaches have been adopted for increasing both the energy density and the power density of lithium ion batteries, and controlling the nanostructure of the electrode material has been one such widely adopted approach.[2]

One-dimensional (1D) nanostructures in particular have received considerable attention for both cathode and anode materials[3–5] due to the several advantages provided by the 1D nanostructures, which can enhance both the energy and the power density of the battery. These advantages include (1) the efficient electron transport pathway provided by the nanostructure,[6] (2) shorter ion diffusion path owing to the less tortuous path and the larger surface to volume ratio,[7] and (3) better strain relaxation due to the accommodation space in between the nanostructures.[8] Recent research has focused on the direct growth of the 1D nanostructures on the current collector to obtain oriented nanostructures which further provide improved performance due to the direct attachment of each 1D nanostructure to the current collector ensuring their participation in the electrochemical reaction and obviating the need for any binding agent.[4,8] Such nanostructures have been demonstrated to outperform powder pressed electrodes or randomly oriented nanostructures for silicon,[4] cobalt oxide,[9] germanium,[8] tin oxide,[10] iron oxide,[11] and titanium dioxide.[12]

Different applications of LiBs demand the optimization of their energy density and power density. While nanostructuring aims to maximize both the densities, further tuning of the nanostructure can be performed to achieve the optimum balance of the energy density and the power density of the battery. Use of electrochemical engineering based models for LiB has been demonstrated in design optimization of LiBs with porous electrodes. First use of these modeling approaches in choosing porosity and thicknesses for a LiB was demonstrated by Newman using reaction zone model[13] and pseudo two dimensional model.[14] Ramadesigan et al.[15] have incorporated ohmic drop in porous electrode to derive optimal porosity distribution. Use of electrochemical models incorporating capacity fade mechanisms has also been used to provide insights into the effect of porosity distribution and tortuosity on Ragone plots for LiBs.[16] Recently, Dai and Srinivasan[17] suggested an approach for improving energy density of a LiB by graded porosity design tool.

However, a fundamental study to understand the effects of the structural parameters of oriented nanostructures on the performance of a battery is lacking. While the abovementioned studies have been focused on the porous electrode made out of smaller particles, the present work focuses on macro-homogeneous modeling approach to quantify the performance of an electrode made out of one-dimensional oriented nanostructures. The objectives of the present work are (1) to study the effect of 1D nanostructure height on the LiB electrode performance, (2) to develop a mathematical model to aid in the understanding of the influence of 1D oriented nanostructure properties on the performance of the LiB and (3) to predict an optimized structure to achieve the best performance LiB for a specific application depending on the desired energy density and the desired rate of charge and discharge. We propose the use of a modified porous P2D model to simulate the role of nanostructure on the high rate electrochemical performance of the TiO_2 anode. This macro-homogeneous model can provide a system level understanding of the coin cell, such as how various resistances (e.g. kinetic resistances, transport resistances etc.) affect the overall battery voltage and battery performance. The model is validated with experimental results obtained for 1D single crystal oriented TiO_2 anode synthesized directly on stainless steel current collector foils using the aerosol chemical vapor deposition (ACVD) process.

Model Description

A P2D (Newman type) model[18] is used to quantify the effects of various transport processes in a porous anode, cathode, and separator. In the present work, the Newman type model (i.e. a macro homogeneous model with concentrated solution theory) is used to describe the dynamics of TiO_2 cylindrical rods as cathode (vs. lithium foil) (Figure 1). There are four variables of interest: electrolyte concentration c, solid phase potential Φ_1, electrolyte potential Φ_2, and solid

*Electrochemical Society Student Member.
**Electrochemical Society Member.
zE-mail: pbiswas@wustl.edu

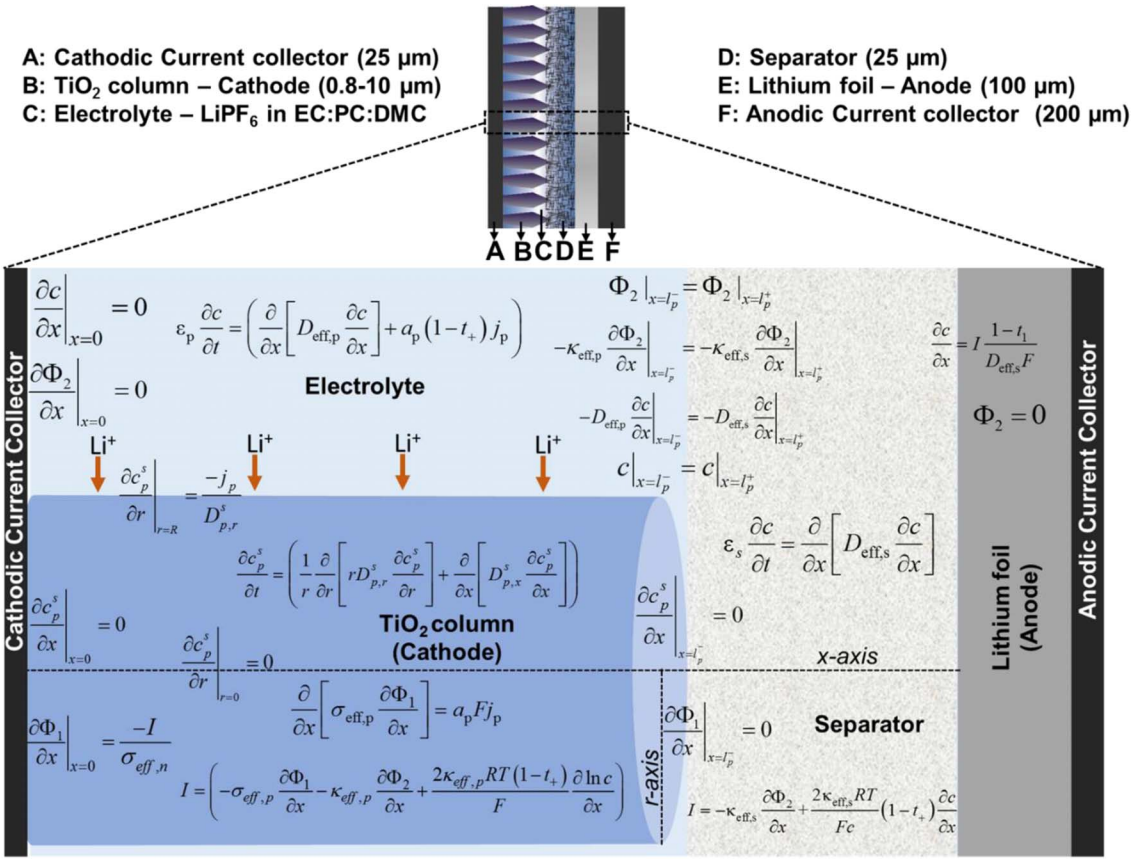

Figure 1. Schematic of the P2D type model for a lithium-ion half-cell with 1D oriented TiO_2 columnar electrode.

phase lithium concentration in cathode c_p^s. Figure 1 shows the equations used to describe the transport and reaction processes. The input parameters needed for the model are listed in Table I.

Second order finite difference formulation is used to discretize the equations. Compared to a porous electrode battery, where the porous structure is assumed to be made up of small spherical particles of anode and cathode materials, here the cathode is composed of continuous cylinders oriented along the x axis (Figure 1). The formulation presented here is general enough to account for the axial and radial direction diffusion in solid rods. The solid phase diffusion equation for cylindrical coordinates is used with appropriate boundary conditions. Intercalation reaction at the cathode-separator interface is ignored due to the large aspect ratio of length to diameter, hence no-flux boundary condition is used for the solid cylinder at the cathode-separator interface. Note that this model uses Fick's law of diffusion in the solid phase, although the actual intercalation mechanism may be different (e.g. core-shell phase change processes). The model described here only gives a system level understanding of how different transport processes affect the overall battery performance of a battery.

Table I. Values of parameters used for the modeling study.

Symbol	Parameter	Positive Electrode	Separator	Negative electrode (Li foil)	Units	Ref.
$Brugg$	Bruggeman coefficient	1.0 (straight columns)	1.5			
a_p	Surface area per volume of electrode	3.429×10^{-8}			m^2/m^3	Calculated
c_0	Initial electrolyte concentration	1000	1000		mol/m^3	Measured
c_0^s	Initial solid phase concentration	469 (1% of $c_{\max}^s$)			mol/m^3	Assumed
$c_{\max}^s$	Maximum solid phase concentration	46,889			mol/m^3	Calculated
D	Electrolyte phase diffusion coefficient	7.5×10^{-10}	7.5×10^{-10}		m^2/s	28
D^s	Solid phase diffusion coefficient	1.76×10^{-15}			m^2/s	21,24
F	Faraday's constant	96487			C/mol	
i_0	Exchange current density			12.6	A/m^2	29
k	Reaction rate constant	2×10^{-11}			m/s	24
l_i	Region thickness	5	25		μm	Measured
R_c	Column radius	87.5			nm	Measured
R	Universal gas constant	8.314			J/mol/K	
T	Temperature	298.15			K	Measured
t_+	Transference number		0.364			
ε	Porosity	0.34	0.55			Measured
κ	Electrolyte phase ionic conductivity	0.1809	0.1809		S/m	30
σ	Solid phase electronic conductivity	2.35×10^{-6}			S/m	Measured

The electrolyte phase voltage at the anode-separator interface is determined by Butler-Volmer kinetics with the exchange-current density of lithium-foil. Continuity relations for concentration and flux are used for lithium ions in the electrolyte phase at the anode-separator interface. Transport in electrolyte phase is considered only in the x direction. Only the solid cylinder is modelled in two directions: axial and radial. Since the cylindrical rods are straight, the tortuosity is assumed to be unity in the cathode. The formulation of P2D model is general enough to take care of any tortuosity in the separator.

The equations used in the model are as follows:

Cathode/current collector boundary conditions.—No mass flux of lithium ions in electrolyte at cathode/collector interface:

$$\left.\frac{\partial c}{\partial x}\right|_{x=0} = 0 \qquad [1]$$

No mass flux of lithium in solid phase at cathode/collector interface:

$$\left.\frac{\partial c_p^s}{\partial x}\right|_{x=0} = 0 \qquad [2]$$

Current is carried by the solid:

$$\left.\frac{\partial \Phi_1}{\partial x}\right|_{x=0} = \frac{-I}{\sigma_{eff,n}} \qquad [3]$$

Zero electrolyte current at the current collector:

$$\left.\frac{\partial \Phi_2}{\partial x}\right|_{x=0} = 0 \qquad [4]$$

Cathode/electrolyte and axisymmetric boundary conditions.—Symmetry boundary condition at column axis:

$$\left.\frac{\partial c_p^s}{\partial r}\right|_{r=0} = 0 \qquad [5]$$

Mass flux at column surface:

$$\left.\frac{\partial c_p^s}{\partial r}\right|_{r=R} = \frac{-j_p}{D_{p,r}^s} \qquad [6]$$

Cathode.—Liquid phase diffusion:

$$\varepsilon_p \frac{\partial c}{\partial t} = \left(\frac{\partial}{\partial x}\left[D_{\text{eff},p}\frac{\partial c}{\partial x}\right] + a_p\left(1-t_+\right) j_p\right) \qquad [7]$$

Solid phase diffusion:

$$\frac{\partial c_p^s}{\partial t} = \left(\frac{1}{r}\frac{\partial}{\partial r}\left[r D_{p,r}^s \frac{\partial c_p^s}{\partial r}\right] + \frac{\partial}{\partial x}\left[D_{p,x}^s \frac{\partial c_p^s}{\partial x}\right]\right) \qquad [8]$$

Solid phase potential flux:

$$\frac{\partial}{\partial x}\left[\sigma_{\text{eff},p}\frac{\partial \Phi_1}{\partial x}\right] = a_p F j_p \qquad [9]$$

Charge balance:

$$I = \left(-\sigma_{\text{eff},p}\frac{\partial \Phi_1}{\partial x} - \kappa_{\text{eff},p}\frac{\partial \Phi_2}{\partial x} + \frac{2\kappa_{\text{eff},p} RT\left(1-t_+\right)}{F}\frac{\partial \ln c}{\partial x}\right) \qquad [10]$$

Cathode/separator boundary conditions.—Mass continuity:

$$c|_{x=l_p^-} = c|_{x=l_p^+} \qquad [11]$$

Mass flux continuity:

$$-D_{\text{eff},p}\left.\frac{\partial c}{\partial x}\right|_{x=l_p^-} = -D_{\text{eff},s}\left.\frac{\partial c}{\partial x}\right|_{x=l_p^+} \qquad [12]$$

No mass flux into top of columns (ASSUMED):

$$\left.\frac{\partial c_p^s}{\partial x}\right|_{x=l_p^-} = 0 \qquad [13]$$

No solid potential flux at top of column:

$$\left.\frac{\partial \Phi_1}{\partial x}\right|_{x=l_p^-} = 0 \qquad [14]$$

Flux continuity:

$$-\kappa_{\text{eff},p}\left.\frac{\partial \Phi_2}{\partial x}\right|_{x=l_p^-} = -\kappa_{\text{eff},s}\left.\frac{\partial \Phi_2}{\partial x}\right|_{x=l_p^+} \qquad [15]$$

Electrolyte potential continuity:

$$\Phi_2|_{x=l_p^-} = \Phi_2|_{x=l_p^+} \qquad [16]$$

Separator.—Electrolyte phase diffusion:

$$\varepsilon_s \frac{\partial c}{\partial t} = \frac{\partial}{\partial x}\left[D_{\text{eff},s}\frac{\partial c}{\partial x}\right] \qquad [17]$$

Charge balance:

$$I = -\kappa_{\text{eff},s}\frac{\partial \Phi_2}{\partial x} + \frac{2\kappa_{\text{eff},s} RT}{Fc}\left(1-t_+\right)\frac{\partial c}{\partial x} \qquad [18]$$

Separator/anode boundary conditions.—Ion dissociation from Li foil:

$$\frac{\partial c}{\partial x} = I\frac{1-t_+}{D_{\text{eff},s}F} \qquad [19]$$

Reference potential:

$$\Phi_2 = 0 \qquad [20]$$

The output of the battery model is the charge/discharge curve for any rate. From these charge/discharge curves, specific capacity (mA.h.g^{-1}) and areal capacity (mA.h.cm^{-2}) are computed for different structural parameters which can aid in deciding the optimal parameters for a given power application.

Experimental

1D Nanostructure synthesis, and cell fabrication.—1D nanostructures were synthesized directly on the current collector by the ACVD process[19,20] as described previously.[21] Briefly, titanium tetraisopropoxide (TTIP) (97%, Sigma-Aldrich, MO, USA) was fed into a reaction chamber toward a heated substrate (current collector). Gas phase reaction and nucleation leads to the formation of TiO_2 particles which deposit onto the heated substrate wherein they sinter to form the 1D nanostructures (columns).[22] The height of the columns was controlled by the varying the deposition time. Stainless Steel (SS316, ESPI Metals, OR, USA) substrates with a thickness of 25 μm and punched into 15 mm diameter discs were used as the current collector. Post deposition, the discs were cleaned to remove any impurity followed by drying in an oven at 85°C for 12 hours. Coin cells (CR2032) were assembled in an Ar-filled glove box (Unilab, MBraun Inc, USA) with O_2 and H_2O concentrations maintained at <0.1ppm levels. The columnar TiO_2 deposited stainless steel discs were used as the working electrode (cathode) and the lithium foil as the counter electrode (anode) in a half-cell configuration.

Electrochemical testing.—Electrochemical characterization of the coin cells was carried out using a multichannel potentiostat/galvanostat (Bio-logic USA, TN, USA) in a potential range of 1.0 V to 3.0 V at a constant temperature of 22°C. The cycling rates were calculated on the basis of 1 Li^+ exchanged per formula unit of TiO_2 in 1 h (denoted 1 C) corresponding to a theoretical capacity of 335 mAh g^{-1}. The mass of the deposited TiO_2 was calculated by weighing the stainless steel discs before and after deposition of TiO_2.

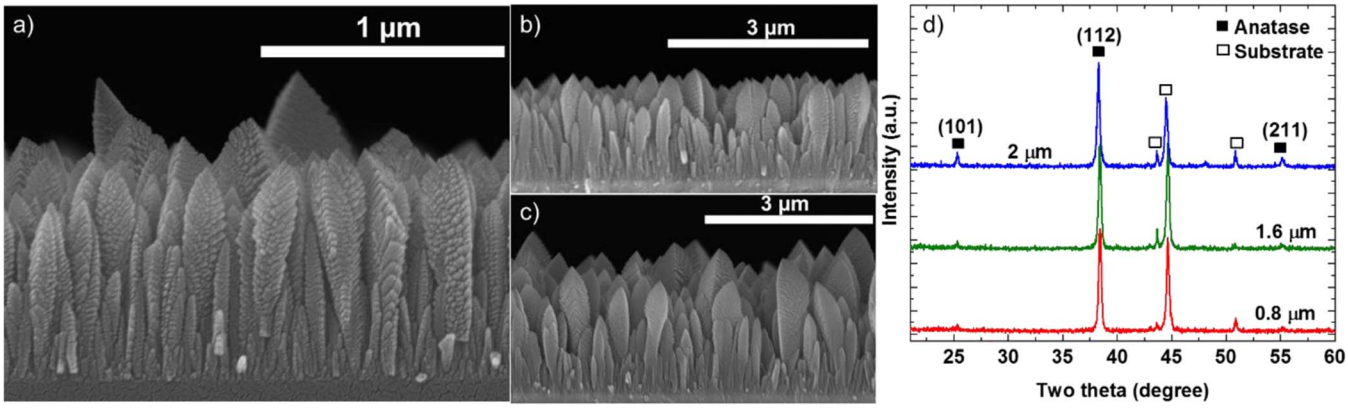

Figure 2. SEM image of the (a) 0.8 μm (b) 1.6 μm and (c) 2 μm columnar nanostructures. (d) XRD spectra of the TiO_2 columnar structures of the different heights.

Structural characterization.—The morphology of the synthesized nanostructures was characterized using scanning electron microscopy (SEM) (FESEM, NOVA NanoSEM 230, FEI Co.). The crystal structure of the prepared sample was characterized using X-Ray diffraction (XRD) (Bruker D8 Advance) with a CuKα radiation (wavelength = 1.5406 Å) at 35 kV and 35 mA. The scattering angle (2θ) used in the measurement was from 20° to 60° with a step size of 0.02° and a dwell time of 2 sec.

Results

Experimental results.—The synthesized 1D nanostructures, observed to be of columnar morphology, for three different deposition time of 30 mins, 60 mins and 75 mins had column heights of 0.8 μm, 1.6 μm and 2.0 μm respectively as measured by SEM analysis (Figures 2a–2c). XRD spectra confirmed the preferred orientation of these columnar structures along the (112) direction (Figure 2d). In our previous study, we have characterized the single crystal nature of these columnar structures.[21] With increasing column height, an increase in the (101) peak intensity is observed in the XRD spectra, indicative of branching in the columnar structures. The branching of columnar nanostructures has previously been studied by our group in detail and has been attributed to the decrease in the tip surface temperature of the TiO_2 nanostructure due to thermal conduction effects as the column height increases.[22,23] This decrease in surface temperature results in a decrease in the sintering rates, thus leading to the formation of a branched structure. The branching of the nanostructures becomes observable by SEM for taller columns with height greater than 5 μm. For the purpose of this study, the branching of the TiO_2 nanostructures has been ignored since the growth of branches was minimal up to the 75 mins deposition time used in the experimental work.

The columns of different heights were cycled at a 1 C (335 $mA.h.g^{-1}$) rate, and the 3rd cycle charge discharge curve is shown in Figure 3a. A significant decrease in the specific capacity was observed with increasing column height. This is expected due to the low electron conductivity of the columns, which would result in electron transport limitation with increase in column height. Similar transport limitations were observed previously for the granular structures compared to the columnar structures.[21] It should be noted that even the tallest column (2 μm) used in the study exhibited better specific capacities than the 0.8 μm granular structures (Figure 3a) studied in the previous study, highlighting the better transport characteristics of the columnar nanostructures, which allow much higher mass loading. Long term cycling of the columns revealed an initial capacity decrease of 8–10 % in the first 10 cycles but stable performance (<10% total decrease) afterwards up to 100 cycles at 1 C rate for all the column heights (Figure 3b). The initial capacity decrease is attributed to the buildup of the SEI layer on the surface of the columns[21] in the initial few cycles resulting in coulombic efficiencies in the range of 90–95% which increases to >99% in the following cycles.

The results above indicate that shorter columns have higher specific capacities and hence more suitable for practical applications; however, areal capacity is also an important factor which governs the size of the battery. Figure 3c shows the areal capacity of the various height electrodes for the 100 cycles. It was observed that the areal capacity increases with increasing column height. While the increase seen in the above data appears to be linear with the height of the columns, there are very few data points to establish a relationship of height with the areal capacity. Hence, we see an inverse effect of column height on the specific capacity and the areal capacity of the battery. This prompts the use of a modelling based optimization to predict the optimum column height for practical applications.

Model input and validation.—The parameters and properties of the one dimensional TiO_2 nanostructures were either measured or obtained from the literature. Table I list the parameters used for this study and the source of the parameter. The diffusion coefficient of the 1 D nanostructures was estimated to be 1.76×10^{-15} $m^2.s^{-1}$ based on data from the cyclic voltammetry reported in our previous study[21] and also agreed with previously reported values in the literature.[24] The electronic conductivity of the TiO_2 columnar nanostructures was measured by four probe measurements and was found to be 2.35×10^{-6} S/m, consistent with the values found in literature for TiO_2.[25] Since these nanostructures are directly synthesized on the current collector and no carbon additive is use, the electronic conductivity of the TiO_2 is directly used.

For the input and validation of the model, data from our previous study was used.[21] The electrochemical performance of the 0.8 μm at 0.1 C rate (33.5 $mA.h.g^{-1}$) served as open circuit potential (OCP) of the battery. The voltage time curve was fitted to a parametrized equation[16] as shown below:

$$\begin{aligned} U(\theta) = {} & 0.14334 \times 10^{-2} + 0.25952\exp(-0.71758\theta) \\ & + .66825\tanh(0.28724\theta - 0.14795) \\ & - 3.68355\tanh(6.27217\theta - 5.34464) \\ & - 3.16496\tanh(15.11589\theta + 0.85263) \\ & - 1.16891\tanh(217.33899\theta - 149.81706) \end{aligned}$$

where $\theta = c^s/c^s_{max}$. Using the above discharge curve at 0.1 C rate, the performance of the 0.8 μm at higher discharge rates (up to 10 C) was simulated. Figure 4a shows the experimental and modelled discharge curves of the TiO_2 column at different discharge rates. It can be seen that the model performs well in simulating the kinetics of the lithium insertion into the TiO_2 nanostructure. However, at very high discharge rate of 10 C, the model deviates from the experimental per-

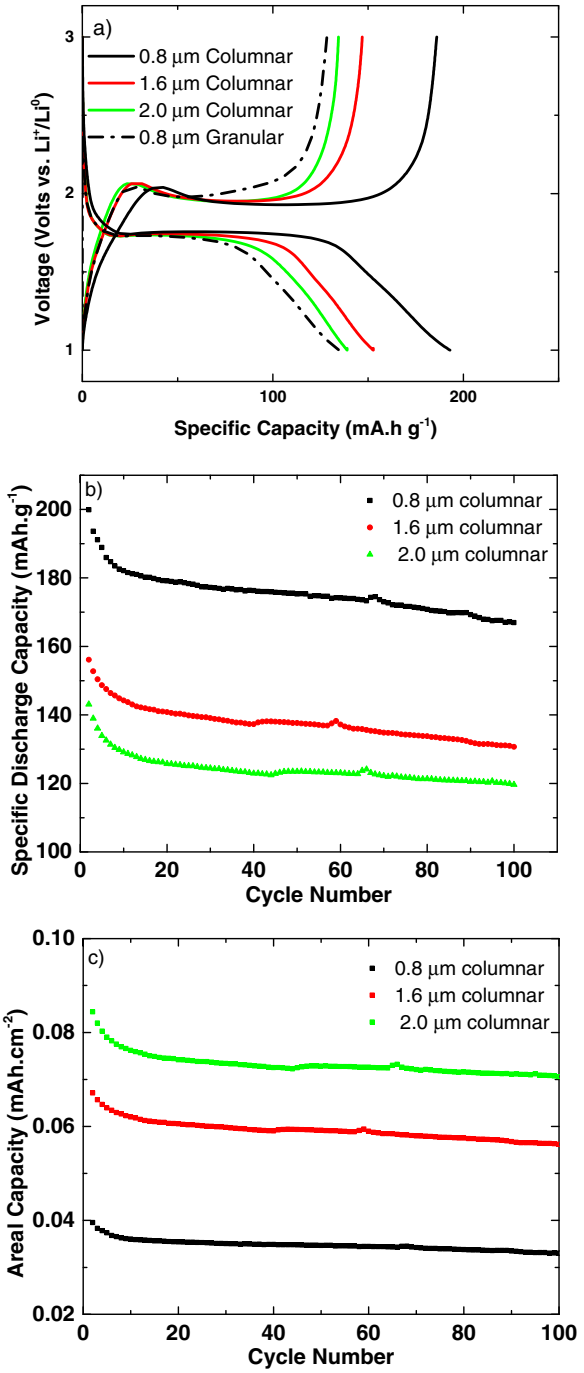

Figure 3. (a) Galvanostatic charge-discharge voltage profiles of columnar nanostructures of varying heights at a 1 C rate of charge and discharge. (b) Cycling performance represented in terms of specific capacity and (c) areal capacity of the columnar structures of varying heights at 1 C rate of charge and discharge.

formance, predicting lower voltage plateau compared to experimental observations. This is possibly due to the simplistic assumption in the model which ignores biphasic ($Li_{0.05}TiO_2$ and Li_xTiO_2) formation and the change in the electronic conductivity and the lithium diffusivity as a result of this biphasic transformation. However, the model still predicts the specific capacity of the electrode at all rates of discharge considerably well, with a less than 5% deviation in the predicted capacity vs. the experimental values. These results validate the ability of the model to predict the performance of the electrodes at varying rates of discharge.

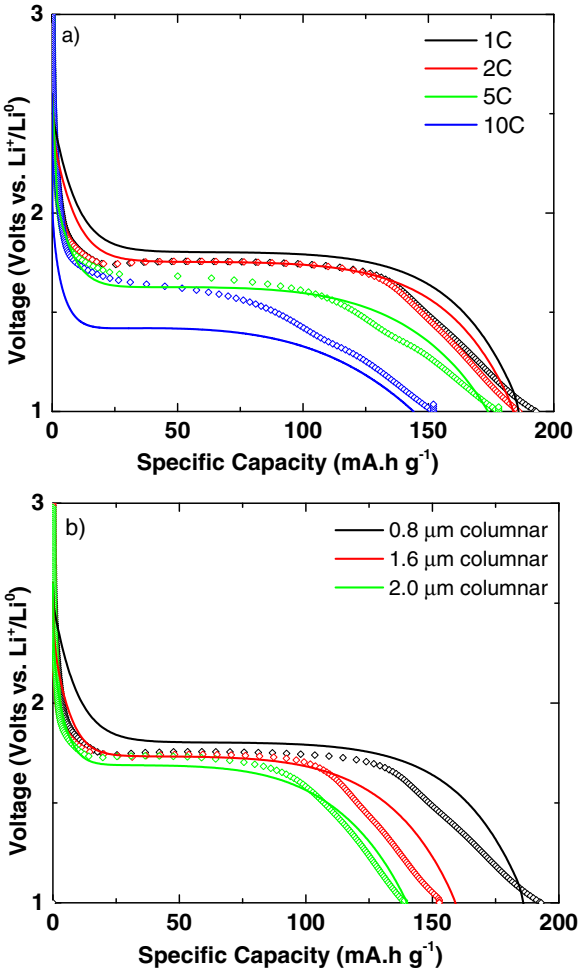

Figure 4. Galavanostatic discharge voltage profile from experimental measurements and modeling of (a) the 0.8 μm columnar nanostructures at varying rates (1 C-10 C) of discharge (intercalation) and (b) the columnar nanostructures of varying heights at 1 C rate of discharge (intercalation). The discrete points represent the experimental data and the model outputs are represented by the solid lines.

The model was then validated against the experimental results obtained for varying column heights reported above. It should be noted that for varying heights, the input to the model is only the OCP relationship obtained from 0.1 C performance of the 0.8 μm columns. Using the same physical parameters of the columns, the mass of the electrode was estimated for taller columns and used in the model. It is seen that the model performs well in predicting the performance of the columnar nanostructures of varying heights (Figure 4b). Again, the difference between the predicted specific capacity and the experimental result is less than 5%. The lowering of the plateau potential is also predicted well by the model, with the predicted plateau potential lowering from 1.81 V to 1.68 V for column height increasing from 0.8 to 1.6 μm. Experimentally plateau potentials range from 1.75 V to 1.70 V for the same increase in column heights.

Understanding the role of transport parameters.—The successful validation of the model allows us to understand the role of transport parameters on the performance of the oriented nanostructured electrodes. Figure 5 shows the effect of diffusivity of lithium in the nanostructure and the electronic conductivity of the columnar nanostructures on the areal capacity of the 0.8 μm height columnar TiO_2 battery electrodes at 1 C and 5 C rates of discharge. The experimentally measured values of diffusivity and conductivity are indicated by

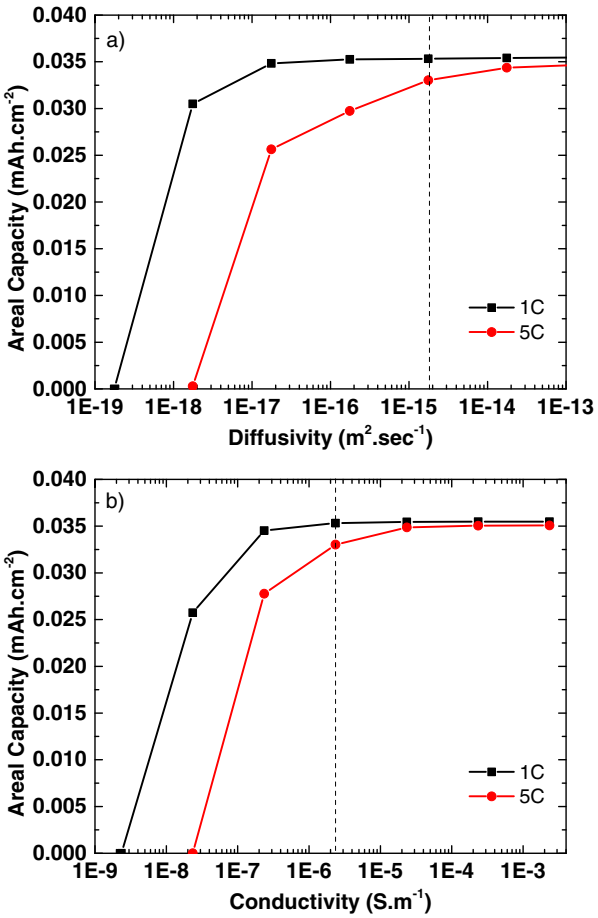

Figure 5. Predicted effect of (a) diffusivity of the lithium in the TiO_2 column and (b) electronic conductivity of the TiO_2 column on the performance of 0.8 μm tall columnar nanostructures. The dashed line indicates the experimentally measured values of the parameters.

the dashed line on the plot. An increase in either conductivity or diffusivity results in better performance of the electrodes, with a saturation point attained at higher values of conductivity and diffusivity. At a 1 C rate of discharge, the electronic conductivity and diffusivity in the 0.8 μm columnar nanostructure is near the saturation performance. However, at a 5 C rate, the performance is not at saturation, and it is seen that both diffusion and electronic conductivity are the performance limiting factors. These results also supports the previous conclusion about poorer performance of granular TiO_2 nanostructures compared to columnar nanostructures being attributed to the lower electronic conductivity and the lithium diffusivity in the granular nanostructures due to the presence of grain boundaries impeding the diffusion rate and electronic conductivity.

Prediction of optimal electrode structures.—In addition to understanding the role of the kinetic parameters, the model's capability in successfully predicting the charge discharge profiles at varying rates as well as varying nanostructure heights, was utilized to predict optimal electrode design strategies. Results above have shown that increase in electrode thickness results in a decrease in specific capacity but an increase in the areal capacity. Using the model, the effect of column height (0.8–10 μm) on the areal capacity was mapped at different rates of discharge (0.1–5 C) (Figure 6). At low rate of discharge (0.1 C), increasing the column height results in an increase in the areal capacity. This increase is evident because at 0.1 C rate, the current density is low (33.5 mA.g^{-1}) and near equilibrium condition exist. Thus taller columns provide more active material for the lithium to intercalate and, without any transport limitation, results in increased

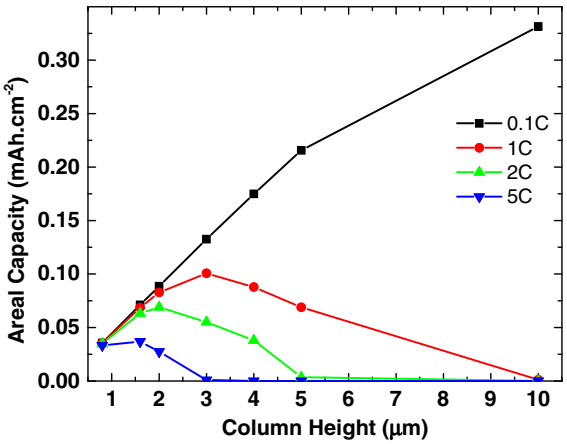

Figure 6. Predicted areal capacity for columnar structures of varying heights at varying rates of discharge.

areal capacities with increasing column heights. However, as the rate of discharge is increased, the effect of transport limitation becomes evident on the areal capacities. At 1 C rate of discharge, the areal capacities increase up to 3 μm column height, above which the areal capacity is observed to decrease rapidly.

The decrease in the areal capacity is mainly due to the lower electronic conductivity of the cathode (nano rods). Simulation results for 3 μm column height at 5 C rate of discharge shows that solid phase conductivity remains the bottleneck. An almost 1 V potential drop occurs between top and bottom of the solid cylinders (Figure 7a) for the conductivity values used for TiO_2. Due to straight pores, the lithium ion concentration in the electrolyte phase remains almost uniform offering little transport limitation. Such maxima or inflection points in the areal capacity vs the electrode thickness have also been reported previously in slurry coated electrodes for lithium ion battery cathodes.[26] Similar to the present study, the inflexion point was observed to shift to lower C rates with increasing electrode thickness.

The P2D model allows us to evaluate performance of battery modified with other materials. For example, addition of conductive carbon to the TiO_2 cylinders can improve the electronic conductivity of the solid phase of cathode. Figure 7b shows the voltage profile for the 3 μm column height at 5 C rate of discharge with an increased conductivity value of graphite (59 S/m) which essentially eliminates the potential drop across the solid phase of cathode. Using the increased conductivity value, significant performance gain in terms of areal capacity can be achieved for the TiO_2 columns as shown in Figure 8a. The inflexion points shift significantly to the right with higher areal capacities. The carbon addition is one way to improve the conductivity of these columnar nanostructures but other ways can also be employed to do similar enhancement in conductivity, such as by doping the nanostructures.[27] On the other hand, similar analysis of performance gain can also be performed by improving the transport limitations during intercalation.

Another morphology factor that can be optimized to obtain high areal capacities is the column –column distance, represented as the porosity of the electrode in the model. Figure 8b shows the effect of the porosity on the areal capacity of an electrode with 10 μm columns with increased conductivity. For the 0.1 C and 1 C rate, the areal capacity is observed to increase with decreasing porosity due to the increasing packing and thus increasing total active material on the electrode. However, for 2 C rate, a maxima is seen for the areal capacity, below which the capacity rapidly decreases. This maxima occurs due to narrowing electrolyte channels between the columns causing transport limitations in the electrolyte phase depending on the rate of discharge. Thus an optimal porosity value for a column of certain height can be obtained depending on the desired rate of discharge. Work done by Suthar et al.[16] on dual porous electrode lithium-ion battery also suggests similar results, where the less porous electrode provides

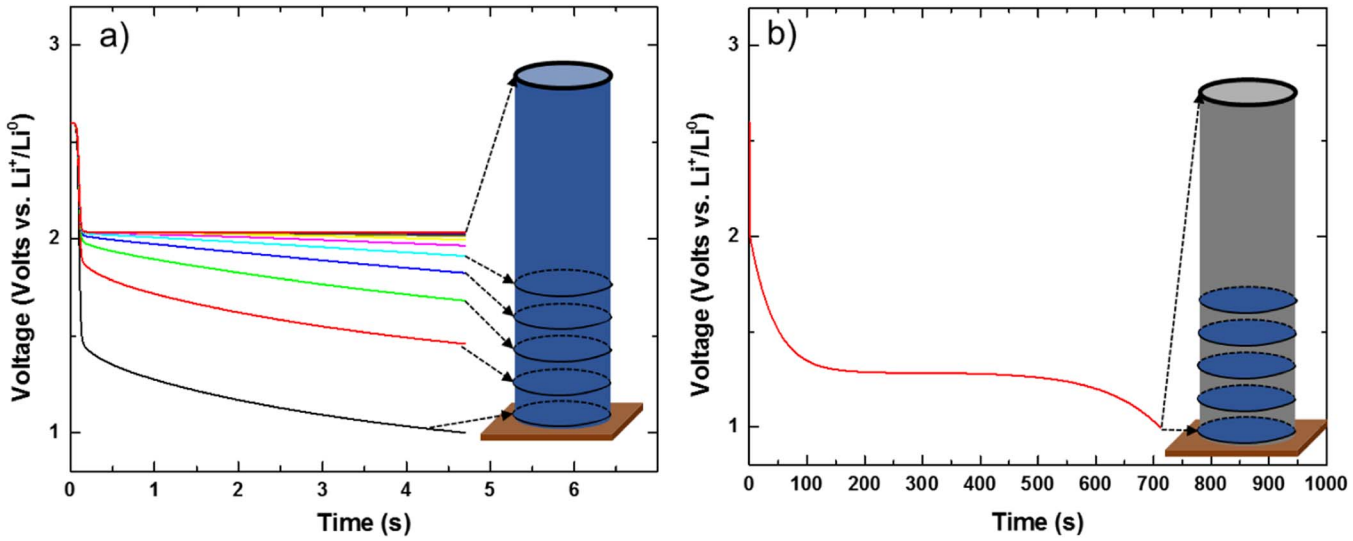

Figure 7. Simulated voltage-time profile at different axial locations in the TiO_2 column for 3 μm tall columns with electronic conductivity of (a) 2.35×10^{-6} S/m (as prepared) and (b) 59 S/m (hypothetical carbon coated electrodes). The different curves are equally spaced on the column in the axial direction.

higher transport resistance in the electrolyte phase leading to reduced specific energy at higher rates of discharge. Although, in that work, porosity also affects tortuosity of electrode whereas in this case, as the tortuosity is taken as unity, porosity only affects the overall lithium ion intake.

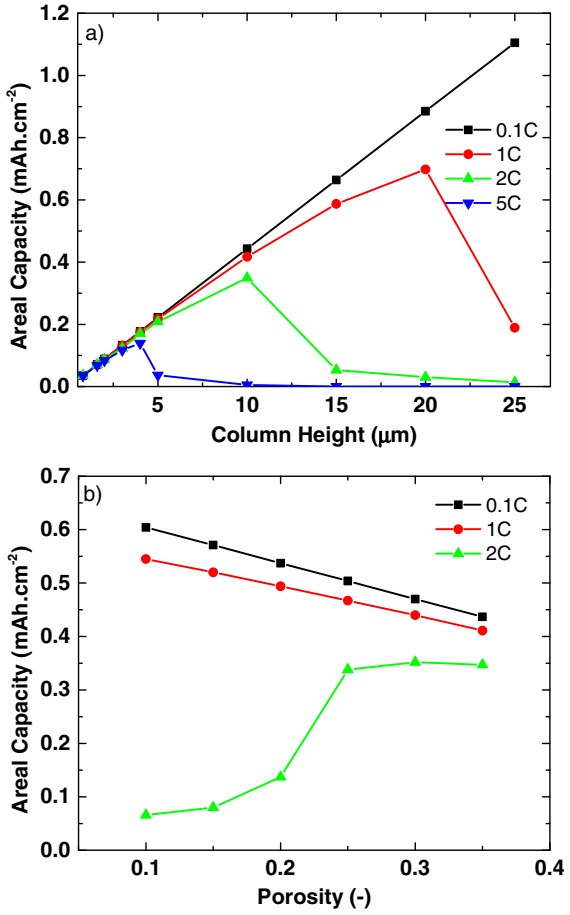

Figure 8. Predicted areal capacity for hypothetical carbon coated columnar structures of (a) varying heights at varying rates of discharge and (b) 10 μm carbon coated columnar structures with varying column spacing (porosity).

Conclusions

One dimensional oriented TiO_2 columnar nanostructures were synthesized and the effect of the column height on the electrochemical performance was studied. An electrochemical P2D model was formulated to predict the performance of 1D nanostructured electrodes in lithium ion battery systems and was successfully validated by the experimental results. The model was utilized to understand the role of kinetic and structural parameters on the electrochemical performance of the TiO_2 columnar nanostructures. Optimal column lengths and column spacing were observed depending on the rate of discharge. Further improvements in the model can be made by considering phase transformation in the solid electrode and radial diffusion in the electrolyte phase. The model can serve as a powerful tool to optimize 1D electrode design for different lithium-ion battery applications depending on the required energy density and the power density and can also be extended to other intercalation based battery applications such as sodium-ion batteries.

Acknowledgments

This paper is based upon work supported under the US-India Partnership to Advance Clean Energy-Research (PACE-R) for the Solar Energy Research Institute for India and the United States (SERIIUS), funded jointly by the U.S. Department of Energy (Office of Science, Office of Basic Energy Sciences, and Energy Efficiency and Renewable Energy, Solar Energy Technology Program, under Subcontract DE-AC36-08GO28308 to the National Renewable Energy Laboratory, Golden, Colorado) and the Government of India, through the Department of Science and Technology under Subcontract IUSSTF/JCERDC-SERIIUS/2012 dated 22nd Nov. 2012. Electron microscopy was performed at the Nano Research Facility (NRF) at Washington University in St. Louis, a member of the National Nanotechnology Infrastructure Network (NNIN), supported by the National Science Foundation under grant No. ECS-0335765.

List of Symbols

Symbol	Description
a_p	Surface area per volume of electrode
$Brugg$	Bruggeman coefficient
c	Electrolyte concentration
c^s	Solid phase concentration
$c^s_{\max}$	Maximum solid phase concentration
D	Electrolyte phase diffusion coefficient

D^s	Solid phase diffusion coefficient
F	Faraday constant
I	Applied current
j_p	Current density gradient flux in electrolyte phase of positive electrode
k	Reaction rate constant
l_i	Region thickness
R_c	Column radius
R	Universal gas constant
r	Radial coordinate
T	Temperature
t_+	Transference number
U	Open circuit potential

Greek

ε	Porosity
Φ_1	Solid phase potential
Φ_2	Electrolyte phase potential
κ	Electrolyte phase ionic conductivity
σ	Solid phase electronic conductivity

Subscripts

Symbol	Description
n	Related to the negative electrode-the anode
p	Related to the positive electrode-the cathode
r	Denotes radial direction
s	Related to the separator
x	Denotes axial direction

Superscripts

Symbol	Description
s	Related to solid phase

References

1. V. Etacheri, R. Marom, R. Elazari, G. Salitra, and D. Aurbach, *Energy Environ. Sci.*, **4**, 3243 (2011).
2. A. S. Arico, P. Bruce, B. Scrosati, J.-M. Tarascon, and W. van Schalkwijk, *Nat. Mater.*, **4**, 366 (2005).
3. L. Ji, Z. Lin, M. Alcoutlabi, and X. Zhang, *Energy Environ. Sci.*, **4**, 2682 (2011).
4. C. K. Chan, H. Peng, G. Liu, K. McIlwrath, X. F. Zhang, R. A. Huggins, and Y. Cui, *Nat. Nanotech.*, **3**, 31 (2008).
5. H.-W. Lee, P. Muralidharan, R. Ruffo, C. M. Mari, Y. Cui, and D. K. Kim, *Nano Lett.*, **10**, 3852 (2010).
6. E. Thimsen, N. Rastgar, and P. Biswas, *J. Phys. Chem. C*, **112**, 4134 (2008).
7. J. Li, W. Wan, H. Zhou, J. Li, and D. Xu, *Chemical Communications*, **47**, 3439 (2011).
8. C. K. Chan, X. F. Zhang, and Y. Cui, *Nano Lett.*, **8**, 307 (2008).
9. Y. Li, B. Tan, and Y. Wu, *Nano Lett.*, **8**, 265 (2008).
10. Y.-D. Ko, J.-G. Kang, J.-G. Park, S. Lee, and D.-W. Kim, *Nanotechnology*, **20**, 455701 (2009).
11. J. Liu, Y. Li, H. Fan, Z. Zhu, J. Jiang, R. Ding, Y. Hu, and X. Huang, *Chem. Mater.*, **22**, 212 (2010).
12. H. Han, T. Song, E.-K. Lee, A. Devadoss, Y. Jeon, J. Ha, Y.-C. Chung, Y.-M. Choi, Y.-G. Jung, and U. Paik, *ACS Nano*, **6**, 8308 (2012).
13. J. Newman, *J. Electrochem. Soc.*, **142**, 97 (1995).
14. T. F. Fuller, M. Doyle, and J. Newman, *J. Electrochem. Soc.*, **141**, 1 (1994).
15. V. Ramadesigan, R. N. Methekar, F. Latinwo, R. D. Braatz, and V. R. Subramanian, *J. Electrochem. Soc.*, **157**, A1328 (2010).
16. B. Suthar, P. W. C. Northrop, D. Rife, and V. R. Subramanian, *J. Electrochem. Soc.*, **162**, A1708 (2015).
17. Y. Dai and V. Srinivasan, *J. Electrochem. Soc.*, **163**, A406 (2016).
18. M. Doyle, T. F. Fuller, and J. Newman, *J. Electrochem. Soc.*, **140**, 1526 (1993).
19. T. S. Chadha, P. Biswas, and W.-j. An, Single-step synthesis of nanostructured thin films by a chemical vapor and aerosol deposition process, in, US Pat. 20,160,056,448 (2016).
20. W.-J. An, E. Thimsen, and P. Biswas, *J. Phys. Chem. Lett.*, **1**, 249 (2009).
21. T. S. Chadha, A. M. Tripathi, S. Mitra, and P. Biswas, *Energy Technol.*, **2**, 906 (2014).
22. T. S. Chadha, M. Yang, K. Haddad, V. B. Shah, S. Li, and P. Biswas, *Chem. Eng. J*, **310**, Part 1, 102 (2017).
23. W.-J. An, D. D. Jiang, J. R. Matthews, N. F. Borrelli, and P. Biswas, *J. Mater. Chem.*, **21**, 7913 (2011).
24. L. Kavan, *J. Solid State Electrochem.*, **18**, 2297 (2014).
25. A. Bally, Electronic properties of nano-crystalline titanium dioxide thin films, in, Citeseer (1999).
26. H. Zheng, J. Li, X. Song, G. Liu, and V. S. Battaglia, *Electrochim. Acta*, **71**, 258 (2012).
27. Y. Furubayashi, T. Hitosugi, Y. Yamamoto, K. Inaba, G. Kinoda, Y. Hirose, T. Shimada, and T. Hasegawa, *Appl. Phys. Lett.*, **86**, 2101 (2005).
28. P. W. C. Northrop, V. Ramadesigan, S. De, and V. R. Subramanian, *J. Electrochem. Soc.*, **158**, A1461 (2011).
29. C. Sequeira and A. Hooper, *Solid State Ionics*, **9**, 1131 (1983).
30. L. O. Valøen and J. N. Reimers, *J. Electrochem. Soc.*, **152**, A882 (2005).